Environmental Science Processes & Impacts

PAPER

View Article Online
View Journal | View Issue

Cite this: *Environ. Sci.: Processes Impacts*, 2019, **21**, 324

Emerging investigator series: radium accumulation in carbonate river sediments at oil and gas produced water discharges: implications for beneficial use as disposal management†

Bonnie McDevitt,[a] Molly McLaughlin,[b] Charles A. Cravotta, III,[c] Moses A. Ajemigbitse,[a] Katherine J. Van Sice,[a] Jens Blotevogel,[b] Thomas Borch[bde] and Nathaniel R. Warner*[a]

In the western U.S., produced water from oil and gas wells discharged to surface water augments downstream supplies used for irrigation and livestock watering. Here we investigate six permitted discharges on three neighboring tributary systems in Wyoming. During 2013–16, we evaluated radium activities of the permitted discharges and the potential for radium accumulation in associated stream sediments. Radium activities of the sediments at the points of discharge ranged from approximately 200–3600 Bq kg^{-1} with elevated activities above the background of 74 Bq kg^{-1} over 30 km downstream of one permitted discharge. Sediment as deep as 30 cm near the point of discharge had radium activities elevated above background. X-ray diffraction and targeted sequential extraction of radium in sediments indicate that radium is likely coprecipitated with carbonate and, to a lesser extent, sulfate minerals. PHREEQC modeling predicts radium coprecipitation with aragonite and barite, but over-estimates the latter compared to observations of downstream sediment, where carbonate predominates. Mass-balance calculations indicate over 3 billion Bq of radium activity (^{226}Ra + ^{228}Ra) is discharged each year from five of the discharges, combined, with only 5 percent of the annual load retained in stream sediments within 100 m of the effluent discharges; the remaining 95 percent of the radium is transported farther downstream as sediment-associated and aqueous species.

Received 27th July 2018
Accepted 21st November 2018

DOI: 10.1039/c8em00336j

rsc.li/espi

Environmental significance

In western U.S. states, billions of liters of oil and gas wastewater are discharged to frequently dry, ephemeral stream beds for beneficial reuse. Elevated sediment radium accumulations at points of discharge were observed though effluents contained relatively low dissolved radium concentrations. Because receiving streams offer little dilution benefit for elevated TDS effluent concentrations, observed coprecipitation of radium with carbonate, and to less extent, sulfate minerals, remain a secondary contamination source after effluent discharges cease. As observed with sediment leaching experiments, storm events could resuspend fine-grained sediment particles to the water column for transport downstream, or acidic rain and solubility changes could alter saturation of carbonate minerals, specifically, allowing radium to remobilize as aqueous species that could be bioavailable.

Introduction

Eighty percent of the United States' produced water brought to the surface during oil and gas (O&G) extraction processes is generated in states west of the 98th meridian.[1] In these western states, produced waters are frequently discharged to surface waters in the O&G fields through the National Pollutant Discharge Elimination System (NPDES) and, according to 40 CFR § 435 Subpart E, permitted for beneficial reuse downstream for irrigation, livestock watering, and wildlife propagation. While there remain effluent limits in place for pollutants, the regulations for consistent self-reporting Discharge Monitoring Reports (DMR) are relatively limited and variable by state and discharge. In arid and semi-arid regions, regional NPDES

[a]*Department of Civil and Environmental Engineering, The Pennsylvania State University, University Park, PA 16802, USA. E-mail: nrw6@psu.edu*

[b]*Department of Civil and Environmental Engineering, Colorado State University, 1320 Campus Delivery, Fort Collins, Colorado 80523, USA*

[c]*U.S. Geological Survey, Pennsylvania Water Science Center, 215 Limekiln Road, New Cumberland, PA 17070, USA*

[d]*Department of Soil and Crop Sciences, Colorado State University, 1170 Campus Delivery, Fort Collins, Colorado 80523, USA*

[e]*Department of Chemistry, Colorado State University, 1872 Campus Delivery, Fort Collins, Colorado 80523, USA*

† Electronic supplementary information (ESI) available. See DOI: 10.1039/c8em00336j

discharges may offer an additional, and in some cases substantial, water resource that can aid in boosting local agricultural economies; however, more research related to human health directly associated with produced water disposal in western regions is needed as ecological impacts to *Daphnia magna* and rainbow trout have been observed.[2–4] In these older O&G fields, with low O&G to produced water ratios, production would likely be economically unviable if produced waters required treatment beyond basic oil–water–gas separation and settling before disposal to ephemeral stream beds.

Depending on geologic formation characteristics, produced waters can be highly saline solutions, causing concern for their discharges to surface waters from centralized waste treatment facilities (CWTs) as exhibited in numerous studies in Pennsylvania and the Eastern US with some observed impacts more than 20 km downstream of the discharge.[5–13] Produced water discharges increase concentrations of dissolved naturally occurring radioactive material (NORM), chloride, boron, fluoride, organic contaminants, and trace metals such as arsenic.[14–16]

Radium, a highly soluble component of NORM found in naturally low concentrations in the environment, is a radioactive alkaline earth metal exhibiting similar environmental behavior to calcium, barium, strontium, and magnesium (Ca, Ba, Sr and Mg) that is known to cause lymphoma, bone cancer, and leukemia at higher concentrations due to the uptake of the radium ion into animal bones and calcium-rich tissues where it then decays.[17,18] Radon, a short-lived daughter product of radium decay, is a radioactive gas known to cause lung cancer.[19] Radium-226 ($t_{1/2}$ = 1600 years) and radium-228 ($t_{1/2}$ = 5.75 years) (^{226}Ra + ^{228}Ra) are the two most persistent radioisotopes of radium, respectively sourced from parent rock material uranium-238 and parent rock material thorium-232. Most states and the EPA regulate ^{226}Ra for O&G produced water disposal to surface water at 2.22 Bq L^{-1} (60 pCi L^{-1}), though the drinking water standard is set much lower at 0.185 Bq L^{-1} (5 pCi L^{-1}) for combined ^{226}Ra + ^{228}Ra.[20,21] Compared to the well-characterized, high salinity Appalachian Basin produced waters with median Total Dissolved Solids (TDS) concentrations of 250 000 mg L^{-1} and median ^{226}Ra concentrations of around 111 Bq L^{-1}, median TDS concentrations in Wyoming formations, mined from the USGS Produced Water Database (https://energy.usgs.gov/), range from 4000 to 10 000 mg L^{-1} with a much lower reported ^{226}Ra concentration of 3.14 Bq L^{-1} in the Niobrara formation produced water.[15,22]

Once discharged, radium often associates with suspended particles and other precipitating ions and accumulates in streambed sediments where the action level according to 40 CFR 192 for ^{226}Ra in the top 15 cm of surface soils in inactive uranium and thorium processing sites should not exceed 185 Bq kg^{-1} (5 pCi g^{-1}) above background concentrations and not exceed 555 Bq kg^{-1} (15 pCi g^{-1}) above background in any 15 cm layer below the surface layer in any 100 square meter area (https://www.ecfr.gov). Combined ^{226}Ra + ^{228}Ra accumulation in sediments 200 times background were noted at the discharge of a brine treatment facility disposing treated produced water with a mean ^{226}Ra concentration of 1.97 Bq L^{-1} to a stream in Pennsylvania with observed radium concentrations 1.5 times background up to 31 km downstream from the discharge in reservoir surface sediments and sediment cores 3 years later.[5,23] Additional facilities in Pennsylvania also showed elevated radium activities at the discharges with mean radium values in sediments from 740 to 7400 Bq kg^{-1}, with much of the activity attributed to conventional O&G brines typically produced from the Appalachian Basin.[13] In a 2015 O&G pipeline fluid spill in Williston Basin, North Dakota sediments contained combined ^{226}Ra + ^{228}Ra, 15–100 times background, depending on the study, though the pipeline fluid concentration was relatively low around 0.33 Bq L^{-1} indicating high potential for radium to continually impact ecosystems long-term as a secondary contaminant source through transport of radium-enriched sediments and subsequent release into aqueous phase.[24,25]

The mobility, bioavailability, and toxicity of radium in the aqueous environment depends on its phase as an aqueous species Ra^{2+}, $RaOH^{+}$, $RaCl^{+}$, $RaCO_3^{0}$, or $RaSO_4^{0}$; sorbed to clays, organic matter, and ferric and manganese oxides; or co-precipitated into sulfate and carbonate minerals.[26] Radium preferentially co-precipitates with sulfate and barium or strontium when supersaturated to form radiobarite (Ba,Ra)SO_4 and radiocelestite (Sr,Ra)SO_4 compared to co-precipitation with supersaturated carbonate minerals.[26,27] Menzie *et al.* (2008) demonstrated the low risk for bioaccumulation and toxicity of radiobarite due to its insolubility.[27] However, once radium in sulfate minerals accumulates with easily transported fine-grained sediments and mobilizes to areas with lower concentrations and anoxic conditions, reduction of sulfate minerals by sulfate-reducing bacteria can release the Ra, Sr and Ba back into solution posing a potential risk for bioavailability of the radium.[28–30] In the Eastern US some produced waters were discharged to streams and the ultimate fate of the radium is unclear.[31] Radium sequestration by partitioning into sulfate solid solutions involving barite ($BaSO_4$) and celestite ($SrSO_4$) is widely reported; however, incorporation of radium into calcium carbonate ($CaCO_3$), strontianite ($SrCO_3$), witherite ($BaCO_3$), and other carbonate phases is less well established.[32–46] Because cations with crystal ionic radii larger than Ca^{2+} can fit well in the orthorhombic structure, aragonite may take up significant amounts of Sr^{2+}, Pb^{2+}, Ba^{2+} and, presumably, Ra^{2+}, compared to rhombohedral calcite, which has low potential for equilibrium partitioning of Sr and Ba.[44,45,47–49] Additional carbonate phases including dolomite, ankerite, magnesite, and siderite exhibit potential for adsorption of low concentrations of Ra^{2+} and Ba^{2+}.[50] Carbonates generally dissolve more readily than celestite and barite suggesting potential for radium re-mobilization to the water column in response to episodic dilution and acidification.[51]

To the authors' knowledge this study is the first temporal and spatial characterization of produced water discharges for beneficial reuse and sediment radium accumulation in the Western US. The study aims to (1) characterize sediment radium accumulation with distance from six discharge sites compared to a background reference site, (2) observe changes in radium concentration with depth in a stream-sediment profile, (3) investigate the adsorption and/or co-precipitation

mechanism(s) controlling radium accumulation in sediments, (4) develop a model that includes solid solution radium minerals to predict the fate and transport of anthropogenic radium, and (5) provide recommendations regarding NPDES 40 CFR § 435 Subpart E based on radium bioavailability potential.

Materials and methods

Site description

Wyoming generates the fourth largest volume of produced water in the United States after Texas, California and Oklahoma with 2.18 billion barrels per year as of 2012 and practices beneficial use of produced water for disposal to surface water.[52] This investigation focused on a large river basin in Wyoming that contains two major perennial rivers (B and C) and a naturally ephemeral tributary (A) (Fig. 1). The precise locations are not disclosed in accordance with access agreements with private land owners. The studied stream systems (A, B and C) include ephemeral tributary segments that drain arid plains where cattle and other wildlife range; the NPDES produced water discharges constitute much of the streamflow in the tributaries. Generally, the stream channels are incised through tertiary and quaternary alluvium colluvium, and fan deposits, which contain gypsum, carbonate, and silicate sediments derived from Cretaceous bedrock in headwaters. Background water and sediment samples were collected from background site UDB-1.0 upstream of all River B NPDES facilities; however, upstream sediment and water samples were not collected from Tributary A and River C NPDES facilities because the NPDES facilities in large O&G fields were the source of the streams. A reference tributary without known O&G development was also sampled west of Tributary A and was mostly dry during sampling events. More detailed site information is included in the ESI.†

In the study area, O&G extraction occurred through wells drilled vertically into reservoirs that have been hydraulically fractured to increase permeability and productivity. The five major reservoirs of oil and gas, from youngest (Cretaceous) to oldest (Pennsylvanian), are the Mesaverde Formation, Nugget Formation, Chugwater Formation, Phosphoria Formation, and Tensleep Sandstone. All NPDES facilities treated produced water similarly with basic oil–gas–water separation (pressure chamber, three phase separator, and heater treater) and a series of settling and skim tank(s)/pond(s) where oil in excess of 1.3 cm depth on the water surface at one facility was removed by vacuum once every two months, before discharge to the otherwise dry, ephemeral stream bed.

Water and sediment sample collection

Water samples were collected during 10 sampling events between 2013 and 2016 at 28 sites. Sampling occurred in May and November 2013, May, July and October 2014, July and October 2015 and June, August and October 2016. Streamflows in the larger Tributary A and Rivers B and C, determined from USGS stream gauges, indicated relatively constant flows during sampling events except for one potential outlier with peak flows during the June 2016 sampling event likely due to heavy snowmelt not captured during other sampling years; more detailed sampling information is included in the ESI.† Specific conductance, pH, temperature, and dissolved oxygen were

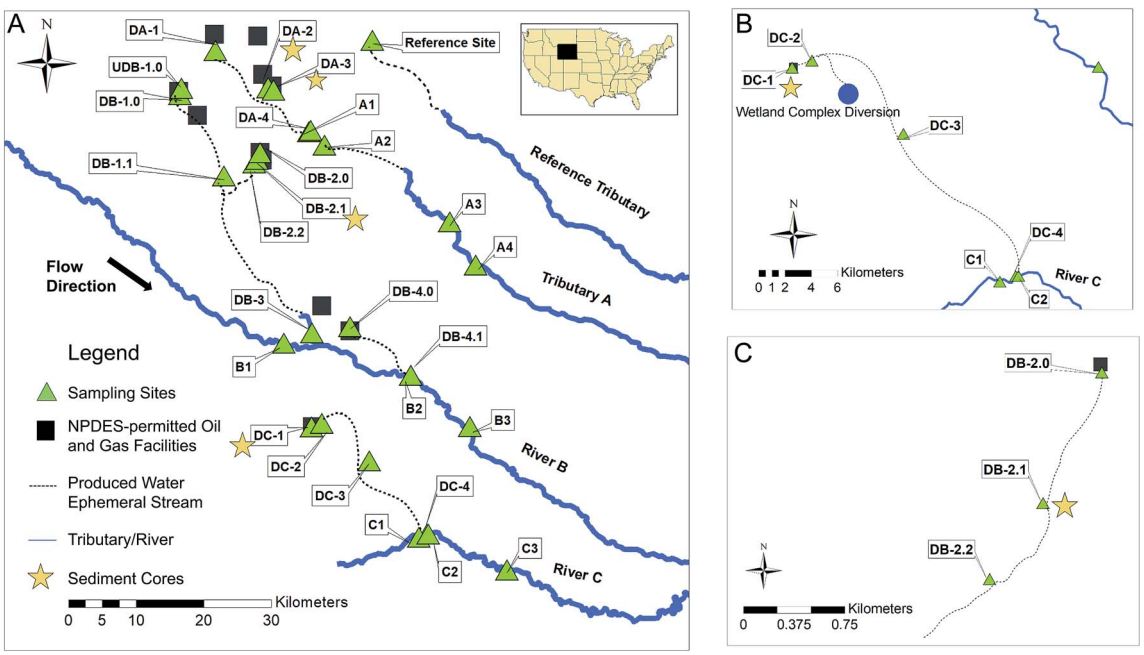

Fig. 1 Locations of water and grab sediment sampling points near NPDES permitted discharges with ephemeral streams, Tributary A, River B, River C and a reference site with no known oil and gas activity or NPDES discharges. Note that all tributaries drain to a drinking water supply reservoir downstream. Discharges where sediment cores were taken are denoted by stars. Detailed maps of the DC-1 (upper right corner) and DB-2.0 (lower right corner) discharges and produced water streams are included.

measured in the field at each location using a Hydrolab field meter. Water samples were field filtered with 0.45 μm pore size cellulose acetate membranes for major anion analysis and then preserved with nitric acid (HNO_3) to pH less than 2 for major cation and trace metal analysis. All samples were stored at 4 °C in the laboratory before analysis.

Grab sediment samples were collected in triplicate from the upper 5 cm of sediment surface during 2 sampling events in August and October 2016. Five 4-inch diameter sediment push-tube cores of varying depths were collected in October 2016 directly at discharge facility DC-1 (34 cm) and 100 m downstream (22 cm), 1 km downstream from discharge facility DB-2.0 (22 cm), and downstream from discharge facilities DA-2 (24 cm) and DA-3 (16 cm). Cores were frozen in the laboratory until analysis. Both grab sediment samples and sediment cores were collected from the sides of the stream channels, avoiding large boulders and rocks, from sediments at the water surface level. If a stream channel meandered, sediments were collected from the point bar side of the bend to capture sediment accumulation.

Water sample analysis

Filtered, acidified water samples were analyzed for major cations by inductively coupled plasma atomic emission spectroscopy (ICP-AES) and ICP mass spectrometry (ICP-MS) for trace metals. Filtered, non-acidified samples were analyzed for major anions by ion chromatography (IC). Samples with major anion/cation charge balances greater than 15% difference were not included in the statistical analysis. Four samples out of 247 total samples (less than 2% of samples) did not meet this criterion, two of which were collected at the reference sample site due to a lack of sufficient available water sample for anion IC analysis.

Dissolved radium-226 activities were analyzed by a modified EPA Eichrom method where radium was coprecipitated with barium sulfate and then analyzed *via* alpha spectrometry.[53] Dissolved radium-228 was measured using a modified EPA RA-05 method with precipitation and analysis *via* beta spectrometry.[54]

Sediment sample and core processing

Sediment samples were dried, ground with mortar and pestle, and sieved to 1.18 mm size fraction to exclude large rocks and organic material. Sediment was then packed into 20 mL high-density polyethylene vials, and sealed with tape to prevent the escape of ^{222}Rn for at least 21 days to allow for establishment of secular equilibrium of ^{226}Ra daughter products (^{214}Pb and ^{214}Bi). Samples were then measured on a Canberra small anode germanium gamma ray spectrometer (SAGe) detector located in the SALTS lab at The Pennsylvania State University. ^{226}Ra activity was reported as the average activity of 351.93, 295.22, and 609.31 keV peaks and ^{228}Ra was measured using the 911.20 keV peak (^{228}Ac). Samples were measured to counting errors less than 5% per peak and background counts were subtracted. A uranium ore tailing standard (UTS-2) from Canadian Certified Reference Material Project with certified activities was used as a calibration standard for detector efficiency calculations in the same vial geometry as samples (http://www.nrcan.gc.ca/mining-materials/). The standard was prepared, sealed, and measured in the same manner as the samples.

Sediment cores were extruded from the casing and sectioned into 4 cm intervals prior to processing. Porewaters were extracted by centrifuge and pH and conductivity were measured immediately. Porewaters were then filtered and preserved to pH less than 2 with HNO_3 for cation analysis by ICP-AES. Sediments were then processed similarly to grab sediments in triplicate for radium measurement. ^{228}Ra measurements were adjusted for the decay since collection by multiplying by the decay constant and adding to the measured value. Additionally, ^{210}Pb was measured through 47 keV and ^{228}Th was measured through the ^{212}Pb peak (239 keV) in order to apply age dating techniques.[55]

Sediment characterization

Selected grab sediment samples from the DC-1 and DB-2.0 produced water streams (DC-1, DC-2, DC-3, C1, C3, reference site, DB-2.0, DB-2.1 and DB-2.2) ($n = 9$) were grain-sized by sieve on a shaker for 15 minutes into three categories: coarse sand (>300 μm), fine sand (<300 μm and >45 μm), and silt + clay (<45 μm). Grain-sized samples were measured on the SAGe for radium measurement and then analyzed on a PANalytical Empyrean X-ray Diffractometer (XRD) and Jade software in the Materials Characterization Lab (MCL) at The Pennsylvania State University for quantitative mineralogy with enhanced resolution. Mineralogy of the total sample was combined using the three known grain-sized masses.

A four step sequential leaching procedure modified from Phan *et al.* (2015) and Stewart *et al.* (2015) was performed on the same grab sediments analyzed for mineralogy ($n = 9$) with a solution to sediment ratio of 20 : 1 to facilitate detection limits of major cations in the leachates.[56,57] The operationally defined procedure used to determine radium speciation was as follows:

(1) Water soluble fraction targeted using ultra-pure distilled water and shaken for 24 hours.

(2) Exchangeable cation fraction targeted using 1 M ammonium acetate buffered to pH 8 with ammonium hydroxide to prevent carbonate dissolution and shaken for 12 hours.

(3) Carbonate fraction dissolved using 8% ultra-pure glacial acetic acid (pH = 2.3) and shaken for 12 hours.

(4) Oxide fraction (*i.e.* iron and manganese oxides) targeted using 0.1 M ultra-pure hydrochloric acid and shaken for 12 hours.

After each leaching step, samples were centrifuged at 10 000 RPM for 10 minutes, leachates were filtered through 0.45 μm pore size nylon filters, and remaining residues were freeze-dried and analyzed on the SAGe for radium activities (adjusted for measurement 1.75 years after sampling). Because leach residues were not incubated for at least 21 days, ^{226}Ra activities were quantified by direct measurement at 186.21 keV following peak deconvolution to correct for ^{235}U interference. After steps 2–4, solid residue was rinsed three times with ultra-pure distilled water, shaken, centrifuged, and filtered to ensure

complete removal of targeted species and the rinse water was recombined with original leachate removed. Leachates were analyzed immediately for pH and preserved with HNO_3 for major cation analysis by ICP-AES. Two leach step 4 residues (DC-1 and DB-2.0) were analyzed by Scanning Electron Microscopy (SEM) and Energy Dispersive X-ray Spectroscopy (EDS) using a FEI Quanta 250 Environmental SEM and Aztec software to observe remaining element associations.

Geochemical modelling of radium

The PHREEQC 3.4.0 aqueous geochemical program was used to compute aqueous and surface speciation and potential for selected minerals to precipitate from the NPDES effluents and associated stream waters.[58] PHREEQC was used with the "phreeqc.dat" data base augmented with thermodynamic data for additional solids from the "wateq4f.dat" data base and for radium species and phases from "sit.dat," both provided with PHREEQC 3.4.0.[59,60] The two radium phases considered relevant for this study, $RaCO_3$ and $RaSO_4$, which are included in sit.dat, utilize thermodynamic equilibrium constants from Langmuir and Riese (1985).[61] In addition to direct output of the mineral saturation index (SI) values for pure phases, SI values for possible carbonate or sulfate solid-solution series containing radium were estimated as the log of the sum of saturation ratios ($SR = IAP/K$) of the components in the solid solution. For example, SI for $(Ca,Ra)CO_3$ solid solution was computed as $\log((a{Ra^{2+}}\cdot a{CO_3}^{2-})/K_{RaCO_3} + (a{Ca^{2+}}\cdot a{CO_3}^{2-})/K_{Aragonite})$, where "$a$" denotes activity of the ion and K is the solubility constant. Aqueous speciation results were also used to estimate the ionic contributions to the specific conductance (SC) in accordance with methods of McCleskey *et al.* (2012).[62] Example PHREEQC codes used for the above simulations and selected graphical results are included in the ESI.†

Although the chemical precipitation of ternary solid solutions such as $(Ba,Sr,Ra)SO_4$ may take place in highly saturated systems and can be modeled using PHREEQC, Zhang *et al.* (2014) reported that the removal of radium by interaction with barite or $(Sr,Ba)SO_4$ were similar, and Rosenberg *et al.* (2018) reported the removal of radium during seawater evaporation could be modeled adequately by chemical precipitation of a binary solid solution of $Ra_xBa_{1-x}SO_4$.[32,42,43,63,64] Furthermore, sampled stream water and sediment cores collected for this evaluation were not in direct contact and, therefore, do not represent equilibrium distributions for the elements. Thus, models considering ternary solid-solutions could not be constrained and were deemed unnecessary for the current evaluation of predominant radium sequestration mechanisms downstream of effluents. Geochemical models presented herewith evaluated potential for the incorporation of Ra^{2+} by solid solutions and its adsorption by hydrous ferric oxide (HFO) and hydrous manganese oxide (HMO), but did not consider the additional potential for its adsorption on carbonate surfaces, which could be important in a system with actively accumulating carbonate minerals.[50]

Results and discussion

Chemistry of produced water discharges, stream water, and stream sediment

Produced water discharge sites generally had higher than background water temperatures, lower than background dissolved oxygen concentrations, and elevated hydrogen sulfide gas levels prompting the use of personal monitors at some sites. Table S1† provides the averages of the major anions and cations of interest with regard to radium coprecipitation, water types, and average field parameters for sites. Generally, TDS concentrations in the produced water discharges were consistent with reported data in the USGS Produced Water Database for Wyoming formations in that they were brackish-type waters and dominated by sodium-sulfate or calcium-sulfate water types, rather than sodium chloride as reported in the Eastern US Appalachian Basin brines.[65] Background river water types were dominated more by calcium-bicarbonate type waters.

TDS, SC, and corresponding solute concentrations for the NPDES effluents and downstream waters collected during 2013–16 indicate two general hydrologic processes in the study area: (1) mixing of relatively elevated TDS effluents with lower TDS stream water, and (2) evaporation of waters along produced water streams until additional mixing with inflows of lower TDS river waters. Downstream trends in solute concentrations and pH (Table S1 and Fig. S1†) are affected by these major processes plus equilibration to atmospheric conditions, mineral precipitation, and other geochemical reactions, as explained below in the geochemical modeling. Linear regressions (R version 0.99.486) of dissolved concentrations *versus* dissolved oxygen concentrations measured along the DC-1 produced water stream indicated that as dissolved oxygen concentrations increased (a surrogate for distance), dissolved SO_4 concentrations increased ($R^2 = 0.508$, $p < 0.01$), dissolved Ba concentrations decreased ($R^2 = 0.65$, $p < 0.01$) and dissolved $^{226}Ra + {}^{228}Ra$ decreased ($R^2 = 0.63$, $p < 0.01$) while dissolved Ca and Sr decreases were not significant.

When compared by sample site, Wilcoxon rank sum statistical tests with conservative Bonferroni corrections indicated River B and C stream system discharges (DC-1, DB-1.0, DB-2.0 and DB-4.0) had significantly higher values for TDS and all major anions and cations ($p < 0.05$) compared to the downstream river sites (C1, C2, C3, B1, B2, B3). Uniquely, Tributary A sample sites (A1, A2, A3 and A4) had significantly higher concentrations for TDS, chloride (Cl), sulfate (SO_4), and sodium (Na) compared to the discharge sites ($p < 0.05$) (DA-1, DA-2, and DA-3). Increased major ion concentrations downstream of the NPDES discharge sites likely result from evaporation and oxidation of hydrogen sulfide downstream.

Dissolved effluent ^{226}Ra values measured during this study were greater than background activities but lower than the 2.22 Bq L^{-1} (60 pCi L^{-1}) effluent limit (Table 1), similar to values reported for effluent from facilities in Pennsylvania that treat O&G wastewater.[31] However, facility DB-2.0, with one measured sample from October 2016, had the highest measured ^{226}Ra value of 1.24 Bq L^{-1}, 62 times the average activity measured at

Table 1 Average TDS and radium activities in water and sediment samples ± standard deviation (SD) collected at each site between 2013–2016. Sites marked with an "x" had average ^{226}Ra activities in sediments more than 185 Bq kg^{-1} (5 pCi g^{-1}) above background

Site Name	TDS (mg L^{-1})	^{226}Ra (pCi L^{-1})	^{226}Ra (Bq L^{-1})	^{228}Ra[a] (pCi L^{-1})	^{228}Ra[a] (Bq L^{-1})	^{226}Ra + ^{228}Ra (Bq L^{-1})	Dissolved ^{226}Ra/^{228}Ra	^{226}Ra (Bq kg^{-1})	^{228}Ra (Bq kg^{-1})	^{226}Ra + ^{228}Ra (Bq kg^{-1})	^{226}Ra + ^{228}Ra (pCi g^{-1})	Sediment ^{226}Ra/^{228}Ra	Fails to meet sediment regulatory limit	# samples dissolved	# samples sediment
A1	1408 ± 193	1.91 ± 0.29	0.07 ± 0.01	2.34	0.09	0.16	1.22	76 ± 18	57 ± 9	134	3.6	0.8		11	6
A2	1271 ± 120	1.29 ± 0.58	0.05 ± 0.02	nd	nd	0.05	nd	68 ± 4	49 ± 15	117	3.2	0.7		11	7
A3	1621 ± 209	nd	nd	nd	nd	nd	nd	41 ± 5	56 ± 11	97	2.6	1.4		11	7
A4	1730 ± 303	0.21 ± 0.10	0.01 ± 0.00	1.13	0.04	0.05	5.37	31 ± 4	36 ± 7	67	1.8	1.2		10	7
DA-1	528 ± 95	4.98 ± 0.74	0.18 ± 0.03	1.31	0.05	0.23	0.26	238 ± 58	77 ± 17	315	8.5	0.3	x	11	5
DA-2	1172 ± 104	4.04 ± 0.56	0.15 ± 0.02	1.18	0.04	0.19	0.29	237 ± 11	63 ± 3	300	8.1	0.3	x	11	7
DA-3	1234 ± 235	9.03 ± 2.66	0.33 ± 0.10	1.40	0.05	0.39	0.15	483 ± 173	100 ± 20	583	15.7	0.2	x	11	7
DA-4	994 ± 191	0.92 ± 1.10	0.03 ± 0.04	2.63	0.10	0.13	2.85	83 ± 29	57 ± 7	141	3.8	0.7		10	11
B1	98 ± 34	0.26 ± 0.11	0.01 ± 0.00	nd	nd	0.01	nd	54 ± 19	362 ± 308	415	11.2	6.7		8	7
B2	106 ± 34	0.27 ± 0.19	0.01 ± 0.01	nd	nd	0.01	nd	30 ± 7	67 ± 19	98	2.6	2.2		8	7
B3	107 ± 38	0.27 ± 0.16	0.01 ± 0.01	1.17	0.04	0.05	4.39	44 ± 6	137 ± 18	181	4.9	3.1		10	7
UDB-1.0	446 ± 179	0.33 ± 0.10	0.01 ± 0.00	nd	nd	0.01	nd	40 ± 3	54 ± 7	94	2.5	1.3		5	7
DB-1.0	6709 ± 3052	0.18 ± 0.10	0.01 ± 0.00	1.14	0.04	0.05	6.39	55 ± 6	53 ± 6	108	2.9	1.0		3	4
DB-1.1	459 ± 190	0.32 ± 0.27	0.01 ± 0.01	1.40	0.05	0.06	4.37	44 ± 3	78 ± 10	122	3.3	1.8		8	7
DB-2.0	3822 ± -	33.40 ± -	1.24 ± -	23.80	0.88	2.12	0.71	2690 ± 130	763 ± 50	3453	93.3	0.3	x	1	3
DB-2.1	5089 ± 965	12.95 ± 2.76	0.48 ± 0.10	5.85	0.22	0.70	0.45	309 ± 79	68 ± 28	378	10.2	0.2	x	2	7
DB-2.2	5264 ± 1164	8.93 ± 1.77	0.33 ± 0.07	2.42	0.09	0.42	0.27	51 ± 4	89 ± 20	139	3.8	1.7		7	7
DB-3	754 ± 333	0.48 ± 0.14	0.02 ± 0.01	nd	nd	0.02	nd	53 ± 2	83 ± 5	136	3.7	1.6		3	7
DB-4.0	5693 ± 874	4.56 ± 1.28	0.17 ± 0.05	3.30	0.12	0.29	0.72	99 ± 3	111 ± 3	210	5.7	1.1		3	4
DB-4.1	1641 ± 884	0.25 ± 0.07	0.01 ± 0.00	1.07	0.04	0.05	4.32	42 ± 14	83 ± 28	125	3.4	1.9		10	6
C1	139 ± 79	0.86 ± 0.35	0.03 ± 0.01	nd	nd	0.03	nd	36 ± 7	35 ± 5	71	1.9	1.0		13	7
C2	144 ± 81	0.79 ± 0.31	0.03 ± 0.01	nd	nd	0.03	nd	62 ± 10	64 ± 13	126	3.4	1.0		13	6
C3	285 ± 157	0.44 ± 0.14	0.02 ± 0.01	nd	nd	0.02	nd	48 ± 9	63 ± 10	111	3.0	1.3		11	10
DC-1	1174 ± 60	7.12 ± 0.72	0.26 ± 0.03	4.38	0.16	0.43	0.62	570 ± 13	279 ± 35	849	23.0	0.5	x	9	7
DC-2	1175 ± 163	6.26 ± 0.69	0.23 ± 0.03	3.28	0.12	0.35	0.52	436 ± 65	183 ± 41	619	16.7	0.4	x	14	12
DC-3	1996 ± 255	1.15 ± 0.48	0.04 ± 0.02	nd	nd	0.04	nd	133 ± 58	81 ± 14	214	5.8	0.6		10	7
DC-4	2054 ± 400	nd	nd	nd	nd	nd	nd	73 ± 4	78 ± 7	151	4.1	1.1		3	4
Reference site	1651 ± 1283	0.47 ± 0.07	0.02 ± 0.00	nd	nd	0.02	nd	52 ± 8	77 ± 17	129	3.5	1.5		5	7

[a] Insufficient number of detectable measurements for SD calculation.

the reference site, and a $^{226}Ra + ^{228}Ra$ measured value of 2.12 Bq L^{-1}, 106 times the average measured at the reference site. These activities were also 212 times the average background water activity of $^{226}Ra + ^{228}Ra$ collected from site UDB-1.0 upstream of all discharges. From DB-2.0 permits, the average $^{226}Ra + ^{228}Ra$ discharged was 0.81 Bq L^{-1} and maximum value was 1.41 Bq L^{-1}. Discharge DC-1 had water $^{226}Ra + ^{228}Ra$ activities 21.5 times higher compared to the reference site and site DA-3 had activities 19.5 times reference.

Though mean dissolved ^{226}Ra and dissolved $^{226}Ra + ^{228}Ra$ activities were greater at all discharge sites in each stream system compared to the river sites and background reference site, activities decreased within a relatively short distance downstream and before confluence points with the larger rivers. For example, the DC-1 produced water stream decreased to around 2 times background water activities of $^{226}Ra + ^{228}Ra$ measured at the reference site within about 15 km downstream of the discharge and 1.2 times background approximately 32 km downstream beyond which the produced water stream frequently dried before reaching and mixing with River C. Within 1 km downstream of DB-2.0, dissolved $^{226}Ra + ^{228}Ra$ activities decreased substantially from 212 times background immediately below the discharge pipe to 70 times; however, activities more than 2 km downstream were still 42 times reference.

While site DB-2.0 discharged produced water with the highest measured dissolved ^{226}Ra and $^{226}Ra + ^{228}Ra$ value in this study, the average reported discharge volume (3.6 L s^{-1}) was a magnitude lower than the facility near DA-3 and two magnitudes lower than DC-1, and facilities near DA-1 and DA-2 (Table S2†). When applying the reported average discharge volumes and measured average $^{226}Ra + ^{228}Ra$ activities from each facility or just downstream, total radium loadings to streams remain hundreds of millions of Bq of activity per year from each NPDES facility. Assuming all discharged radium was sediment associated with a constant porosity on a dry weight basis and homogeneously distributed, a basic mass balance calculation assuming a control volume of 30 m^3 (1 m wide stream, 0.30 m deep, and 100 m long) and sediment density of 1.2 g cm^{-3} using the DC-1 average discharge volume (52.1 L s^{-1}) and measured average total dissolved radium (0.43 Bq L^{-1}), leads to sediment activity of approximately 19 400 Bq kg^{-1} – much more than measured sediment activities of around 925 Bq kg^{-1}. According to this calculation, observed values indicated that less than 5% of annually discharged effluent radium remains in sediment within 100 m of the discharge, though the actual percent is most likely much lower due to many years of Ra loading not considered here. Thus, the radium is either transported with surface or groundwater in either dissolved or particle associated form which could have implications for both human and ecological health depending on its ultimate fate downstream as sorbed, precipitated, or aqueous species.

Sediment radium activities followed similar trends to the dissolved $^{226}Ra + ^{228}Ra$ activities in the water with much larger activities measured at discharge facilities as compared to background and river/tributary sites and decreasing activities with increasing distance downstream (Table 1 and Fig. 2A, 3A and 4A). Ratios of $^{228}Ra/^{226}Ra$ *versus* distance from the discharge were also plotted (Fig. 2B, 3B and 4B). Discharge sites DA-2 and DA-3 had significantly higher $^{226}Ra + ^{228}Ra$ sediment activities compared to all downstream Tributary A sites ($p < 0.05$) with 4.5 and 8.6 times activities at the most downstream Tributary A site, A4, respectively. Tributary A sites, when compared to furthest downstream site A4, remained significantly higher ($p < 0.05$) at sites A1 and A2 until A3, a distance of 60 km downstream of the produced water stream confluence, where there was no significant difference with site A4 activities. DC-1 had significantly higher $^{226}Ra + ^{228}Ra$ sediment activities ($p < 0.05$) than the reference site (6.6 times) and produced water stream sites DC-3 and DC-4 (Fig. 3A). DB-2.0 sediment $^{226}Ra + ^{228}Ra$ activities (Fig. 4A) were 26.7 times reference site sediments and 51.8 times reference ^{226}Ra activities, consistent with findings from the Williston Basin pipeline fluid spill where dissolved radium activities were relatively low around 0.33 Bq L^{-1} but sediments accumulated much of the radium.[24,25] However, as with dissolved Ra activities, DB-2.1 approximately 1 km downstream remained only 2.9 times reference site sediment $^{226}Ra + ^{228}Ra$ activities and 5.9 times reference site sediment ^{226}Ra activities. According to action level threshold 40 CFR 192 for the upper 15 cm of soil, sediment activities should not exceed 185 Bq kg^{-1} (5 pCi g^{-1}) above background – for which all NPDES facilities in this study exceeded as well as produced water stream sites DB-2.1 and DC-2.

Ratios of $^{228}Ra/^{226}Ra$ in sediment samples *versus* distance from the discharge were plotted for DA-1 (Fig. 2B), DC-1 (Fig. 3B)

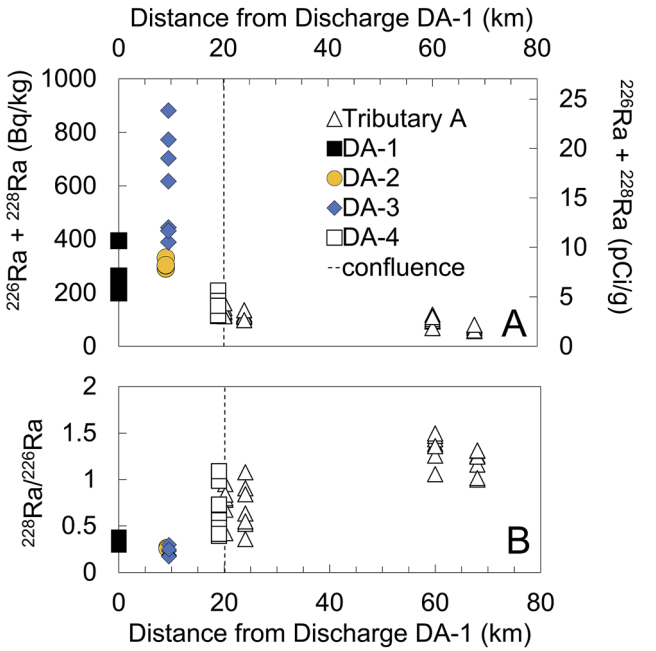

Fig. 2 (A) Total radium activities ($^{228}Ra + ^{226}Ra$) (Bq kg^{-1}) in sediment samples *versus* distance downstream of NPDES discharge DA-1 (black squares). Note additional NPDES discharges at 9–10 km: DA-2 (circles), DA-3 (diamonds), and downstream site DA-4 (open squares). Activities are most elevated near the NPDES discharges and then are mixed and diluted downstream of the confluence with Tributary A. (B) $^{228}Ra/^{226}Ra$ in sediments increase downstream of discharges to reflect mixing with background activities.

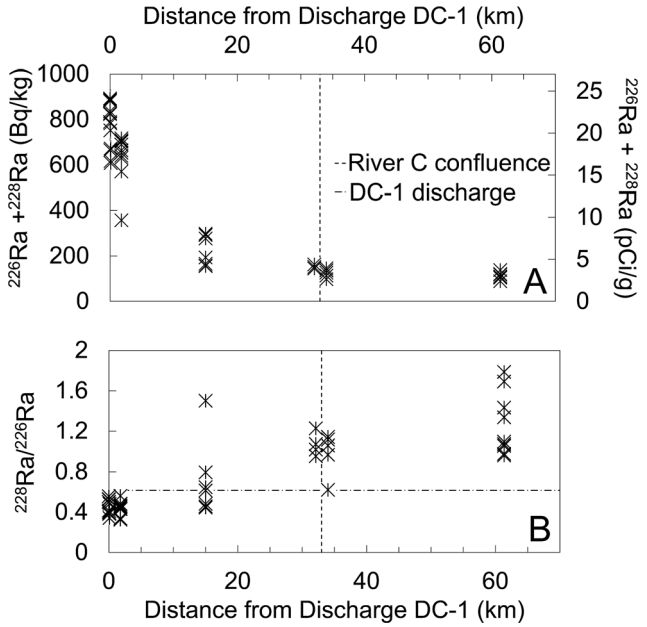

Fig. 3 (A) Total radium activities (^{228}Ra + ^{226}Ra) (Bq kg^{-1}) in sediment samples *versus* distance downstream of NPDES discharge DC-1. Activities are most elevated at the NPDES discharge and then are mixed and diluted downstream of a confluence with River C. (B) ^{228}Ra/^{226}Ra in sediments increase downstream of discharges and are lower in the sediment than the liquid discharge effluent with a ratio of 0.61, indicating accumulation of radium over a period of time. Farther downstream the ratios are high as the impacted sediments mix with background sediments with higher ratios.

and DB 2.0 (Fig. 4B) with a horizontal dashed line indicating the ratio of the NPDES produced water fluid (*i.e.*, effluent). Once the ^{226}Ra and ^{228}Ra are separated from parent material by chemical precipitation and deposition in the stream both radioisotopes will decay with a rapid decrease in ^{228}Ra compared to ^{226}Ra, because of the difference in half-lives. The initial ratio can help fingerprint sources of contamination and, in this case, indicate higher ^{226}Ra in the produced water than natural background ^{228}Ra. Reference site ^{228}Ra/^{226}Ra in sediment ranged from 1.3–1.7, with an average of 1.5 (Table 1), while sediments at sampled discharges (DA-1, DC-1, and DB 2.0) had ratios below 1 with an excess of ^{226}Ra, which often indicates O&G contamination. ^{228}Ra/^{226}Ra ratios increase with distance downstream as ^{226}Ra activities mix with natural sediments and activities return to background levels (Fig. S3†). Interestingly, upstream River B site B1 had very low ^{226}Ra activities but average sediment ^{228}Ra/^{226}Ra of 6.7 (Table 1) was the highest measured in the study indicating high ^{228}Ra relative to ^{226}Ra (average sediment ^{228}Ra activities were 4.7 times reference site ^{228}Ra activities). Site B1 was located downstream of a major agricultural irrigation diversion and dam on River B. Studies have reported higher ^{228}Ra flux from fine-grained, non-carbonate sediments with higher parent material ^{232}Th and increased rates of porewater exchange through sediment turbidation and agricultural associated radium in phosphate fertilizers.[66,67]

Long flow distances in combination with wetland complexes and stock ponds kilometers downstream from NPDES facilities were not sampled during this study, but may provide buffering as produced water streams reach equilibrium temperatures and concentrations prior to mixing with the larger rivers. Despite this benefit, accumulation of the evaporated salt, mineral precipitates, hydrocarbon compounds, and radium in sediments may potentially occur and impact endangered regional wildlife and migratory birds using the O&G produced water created wetlands as stopover habitat as evidenced in bioaccumulation of these components in bird bones studied in Wyoming.[68] The radioactive scaling and precipitates accumulating in sediments may pose long-term secondary sources of contamination to freshwater long after produced water discharges have ceased and potentially impact freshwater biota such as freshwater mussels that were observed to bioaccumulate metals associated with O&G produced water in Pennsylvania streams.[69]

Changes in radium activity with depth of sediment

Sediment radium activities were analyzed with depth to both help quantify the extent of radium accumulation in the streambed and assess possible implications for groundwater. The cores collected at sites DA-2 and DB-2.1 show little change in ^{226}Ra activity with depth compared to surface grab samples which ranged from 44–62 Bq kg^{-1} (Fig. 5A). DC-1 ^{226}Ra activities peaked at 925 Bq kg^{-1} (~19 times background) at a depth of 18 cm while DC-1 100 m and DA-3 peak at 10 and 12 cm

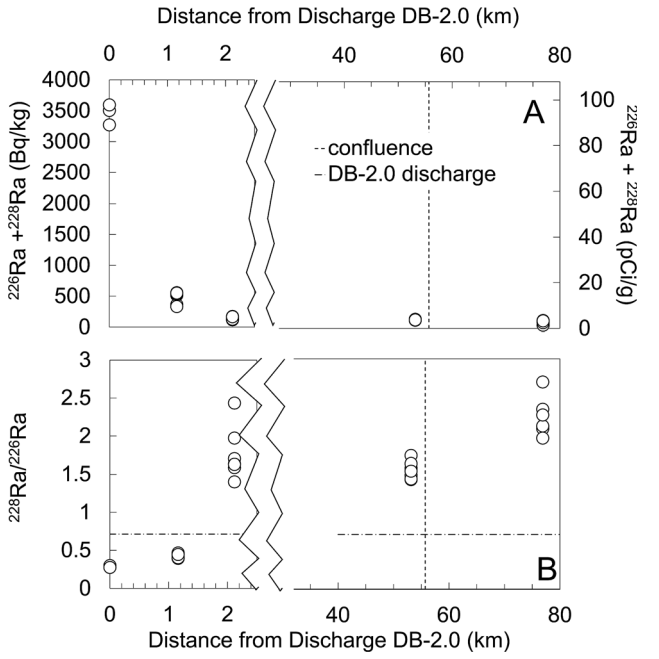

Fig. 4 (A) Total radium activities (^{228}Ra + ^{226}Ra) (Bq kg^{-1}) in sediment samples *versus* distance downstream of NPDES discharge DB-2.0. The highest study activities were measured at DB-2.0 but quickly decrease to near background within 2 km downstream. (B) ^{228}Ra/^{226}Ra in sediments increase downstream of discharges and are lower in the sediment than the liquid discharge with a ratio of 0.71, indicating accumulation of radium over a period of time. Farther downstream the ratios are high as the impacted sediments mix with background sediments with higher ratios.

respectively. The shapes of the activity profiles remain the same when considering ^{226}Ra + ^{228}Ra except that they shift towards higher activities (Fig. S4†). Core radium activities did not decrease to background grab sediment activities even at depth. When observing ^{228}Ra/^{226}Ra ratios with depth all core sites have ratios less than the reference site grab sediment ratio of ~1.5 though DA-2 rapidly approaches background ratios at a depth of around 8 cm (Fig. 5B). The low ^{228}Ra/^{226}Ra ratios compared to background reflect the low Th/U ratio in the O&G formation and the decay of the short-lived ^{228}Ra can be observed at the depth of the ^{226}Ra peak in the DA-3, DC-1 and DC-1 100 m profiles. Assuming consistent sedimentation rate and a deep enough sample to remain unaffected by current radium deposition, a ^{228}Th/^{228}Ra age dating technique was applied to the DC-1 core peak at 18 cm depth, as described by Lauer and Vengosh (2016), and the sediment age was estimated to be 5 years.[55]

When considering the action level for uranium and thorium mill tailings and using the reference site maximum measured ^{226}Ra sediment activity of 65 Bq kg^{-1} (compared to average of 52 Bq kg^{-1}), the regulatory limit for the upper 15 cm of soil is 250 Bq kg^{-1} and the limit below 15 cm is 620 Bq kg^{-1}. Sites DA-2 and DB-2.1 meet both regulatory criteria (Fig. 5A). Sites DA-3, DC-1 and DC-1 100 m fail to meet the regulatory limit in the upper 15 cm and DC-1 additionally fails to meet the below 15 cm regulatory limit. As with radium activities rapidly decreasing with distance downstream from the discharge, DC-1 100 m core also reflects lower activities with depth within a short distance downstream from the discharge pipe. Though DB-2.1 was collected in a wetland-like holding pond around 1 km downstream of the highest measured radium activities in the study at DB-2.0, the radium activities with depth were below regulatory standards indicating the rapid attenuation of radium away from the point of discharge.

Porewater major cation concentrations for each sediment core were observed for changes with depth (Table S3†). Fig. S5† shows the DC-1 porewater concentrations with depth and a distinct peak in manganese concentrations of 120 ppb around 22 cm in depth – in coordination with ^{226}Ra peaks at the same depth. Ra is known to sorb readily to manganese and iron oxides, though manganese oxide is often shown to preferably sorb Ra.[31] Iron concentrations taking method detection limits into consideration, were non-detectable, though Fe(III) precipitation is likely to occur at the porewater pH between 7 and 9 in conjunction with very low (non-detectable) porewater iron concentrations. Ca concentrations remained high throughout the DC-1 core with a small peak around 20 cm in depth and low Ba concentrations as much as 3 orders of magnitude less than Ca concentrations. The manganese concentration peak at depth, consistently high calcium concentrations, and barium concentrations that approach limits of detection in the porewater provide interesting insight into the potential geochemical controls on Ra associations in O&G systems where low Ba concentrations could inhibit the well-studied precipitation of recalcitrant barite minerals and instead allow sorption of Ra with manganese oxides, or coprecipitation with calcium carbonate minerals to become the dominant Ra sequestration mechanism(s).[5,32,33]

Mechanisms controlling radium accumulation in sediment

Modeling progressive evaporation and chemical precipitation of solid solutions downstream of discharges can generally explain the observed downstream trends (Fig. S6†). Conservative evaporation of discharges DB-2.0 and DC-1 adequately explains the observed increases in SC and concentrations of TDS, Cl, and, to a lesser extent, SO_4 and Sr downstream of the discharge, but fails to explain the observed changes in pH and

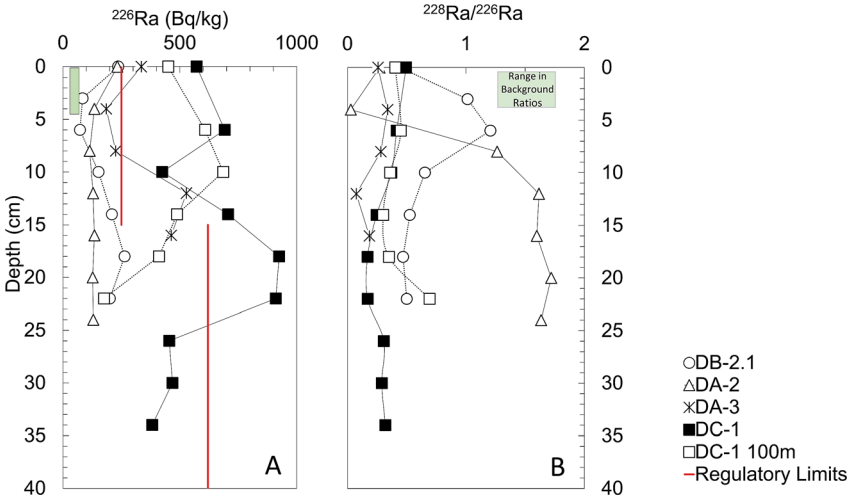

Fig. 5 (A) ^{226}Ra activities (Bq kg^{-1}) *versus* depth in sediment cores collected near the points of NPDES permitted discharges DB-2.0, DA-1, DA-2, DA-3 and DC-1 and 100 m downstream of DC-1. Three of the 5 cores contained sediment activities above the 0–15 cm standard acceptable level above background, while only 1 core, DC-1 appeared to contain sediment above the acceptable activity >15 cm below the sediment–water interface. The reference site grab sediment ^{226}Ra activity ranged from 44–62 Bq kg^{-1} (green bar) in the upper 5 cm. (B) Core DA-2 appeared to have little elevated activity and ratios similar to background sediments at depths greater than 15 cm. However, most cores appear to show decreased $^{228/226}$Ra ratios commonly found associated with older oil and gas wastes. The reference site grab sediment ratio (green square) ranged from 1.3–1.7 in the upper 5 cm.

concentrations of Ca, Ba, and Ra (Fig. S7A, C, E and S8A, C, E†), whose concentrations are less than predicted by simple evaporation. However, the model that combines evaporation with geochemical reactions, including equilibration with the atmosphere and chemical precipitation of $(Ca,Ra)CO_3$ and $(Ba,Ra)SO_4$ solid-solutions, effectively simulates the observed changes in pH, Ca, and Ra, including the general trends for Ba (Fig. S7B, D, F and S8B, D, F†). The equilibrium model over predicts the removal of Ba; observed concentrations are supersaturated with respect to barite and associated solid solutions. Additional simulations indicated that (1) increasing barite solubility by 0.5 log units or (2) adsorption of Ba and Sr by 100 mg L^{-1} each of HFO and HMO had a negligible effect on the potential for Ba or Ra attenuation or associated mineral precipitation. Although large additions of HMO sorbent have been shown to effectively bind Ba and Sr, which decreases the corresponding saturation states for minerals such as barite and celestite, our porewater data indicate very low concentrations of Fe and Mn in the stream sediments (Table S3†) and, thus, do not support modifications to the model that enhance adsorption by HFO or HMO.[31]

Based on modeling results, radium attenuation resulted from its coprecipitation with both aragonite and barite, as $(Ca,Ra)CO_3$ and $(Ba,Ra)SO_4$ solid solutions, respectively. In both modeled cases, the estimated mole fraction of $RaCO_3$ in $(Ca,Ra)CO_3$ was 4 to 6 orders of magnitude less than the corresponding mole fraction of $RaSO_4$ in $(Ba,Ra)SO_4$ (Fig. S9C and D†). Nevertheless, the estimated mass of $(Ca,Ra)CO_3$ precipitated was approximately 3 orders of magnitude greater than that of $(Ba,Ra)SO_4$ (Fig. S9A and B†). Thus, the indicated removal of radium with aragonite and the relative abundance of the carbonate phase in the precipitated solids would be substantial, as indicated by XRD of sediments (Fig. 6). The evaporation models overpredict the removal of barium compared to measured concentrations, thus, the computed mass of $(Ba,Ra)SO_4$ precipitated and the corresponding fraction of radium removed with the sulfate solid-solution phase were overpredicted. Consequently, removal of radium with the carbonate phase may be underpredicted, as the aqueous radium would be available to precipitate as $(Ca,Ra)CO_3$.

We compared the predicted model results to observations of mineralogy in sediments using XRD. Though barite, strontianite, and celestite were indicated to be supersaturated (Fig. S6†), XRD results (Fig. 6) detected only small percentages by weight of less than 5% each of strontianite and barite in the fine sand and silt + clay fractions respectively in sample DB-2.0. Ewaldite $(Ba,Ca(CO_3)_2)$ and strontianite represented <5% and 11% each of the fine sand and silt + clay fractions of sample DB-2.1. However, when the grain-sized results (Table S4†) combined to form the total sample mineralogy, the barite, ewaldite, and strontianite comprised no more than 1% of the total sample by weight. Dolomite was present in many of the samples with substantial compositions in samples DB-2.0, DB-2.1 and DB-2.2 with respective compositions of 7, 9 and <5%. Background samples were more heterogeneous in mineral and clay composition than were DB-2.0 and DC-1 discharge sediments and subsequent produced water stream sites. Discharge site DC-1 was almost completely calcium carbonate dominated (>99%), including both calcite and aragonite, with minor quartz (<1%). Calcium carbonate content decreased with distance downstream from the discharge to DC-3 to where none was detected. DB-2.0 also had a high composition of calcium carbonate (63%) at the discharge though more diversity in carbonate, sulfate, and silicate minerals than DC-1. Background sediments at the reference site contained much more clay and silicate minerals than carbonates and sulfates. Linear regressions on the bulk sediment sample for total $^{226}Ra + ^{228}Ra$ *versus* percent by weight calcium carbonate were weakly significant ($p = 0.09$) for all samples; however, for the DC-1 produced water stream alone ($n = 3$ and thus not statistically relevant) the R^2

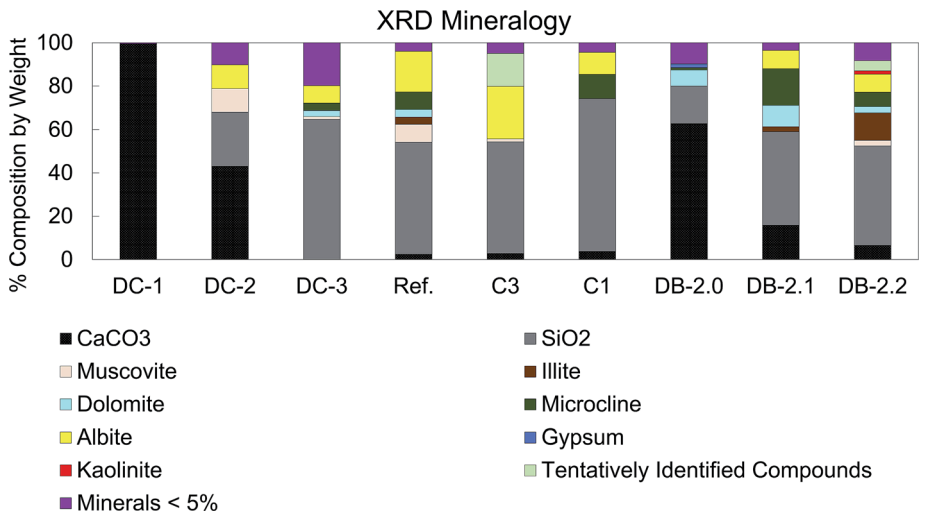

Fig. 6 XRD results for select sediment grab samples. The composited sediments contained predominantly calcium carbonate (calcite and aragonite) or silica (quartz), with an array of minor percentages of other minerals, including no more than 1% barite, ewaldite, and strontianite. Note that the sediments sampled at discharge facilities contained greater percentages of calcium carbonate and lower percentages of quartz compared to background and reference sites.

associated with increasing radium activity and increasing calcium carbonate composition by weight was 0.97. ^{226}Ra + ^{228}Ra *vs.* percent by weight clay mineral compositions were not significant ($p > 0.05$).

Sediment leaching was completed to better understand radium association with operationally defined solid phases. Only the reference site sample lost more than 8% of the total ^{226}Ra activity after the first leach step targeting soluble salts (~20% loss) (Fig. 7). Leach step two targeting exchangeable ions on clay minerals produced varied results, with DC-1, DC-2 and DB-2.0 samples still maintaining over 80% of the total ^{226}Ra activity while River C sites and other produced water sites downstream lost larger percentages of ^{226}Ra activity. Muscovite, detected by XRD at high percentages in some samples can sorb large amounts of Ra while quartz and other silicate mineral compositions of sediments absorb less, confirming that background samples with high quartz compositions preferentially sorb Ra to clay minerals during accumulation.[70,71] Additionally, Ra adsorbed to carbonate surfaces could potentially desorb during this step.[50] Sample DC-1 lost approximately 75% of the total ^{226}Ra activity and 97% of total sample mass after the third leaching step with acetic acid targeting carbonate minerals. This was expected with DC-1 composed approximately 100% of calcium carbonate minerals. DC-2 lost about 70%, DB-2.0 63% and DB-2.1 approximately 42% of total ^{226}Ra activity after the third leach. It is important to note that application of acetic acid in step 3 could have promoted desorption of Ra from iron and manganese oxides, which would otherwise dissolve in HCl during step 4. Leachate chemistry results (Table S5†) demonstrate that Mn and Fe were partly mobilized during the acetic acid step 3. However, the calcium concentrations in step 3 leachates were three orders of magnitude larger than iron and manganese concentrations, and proportionally greater amounts of manganese and iron than calcium were released during step 4. Combined, the leaching results indicate that the majority of radium is likely coprecipitated with calcium carbonates at the NPDES discharges, with smaller fractions associated with iron and manganese oxides, all of which could release radium to waters with low pH. To confirm complete carbonate dissolution, leachates from samples DC-1 and DB-2.0 accounted for 99% and 96% of the sample calcium, respectively. Sample DC-1 only lost 1% ^{226}Ra after leach step four though DB-2.0 lost approximately 8% and downstream sites lost between 10–15% to the acid soluble fraction including Fe and Mn oxides. SEM and EDS elemental mapping for DC-1 and DB-2.0 leach four residues (Fig. S11 and S12†) show no visible association between Sr, Ca, or S with little to no Ba present. Sr present in DB-2.0 residues were likely associated as exchangeable ions on clay particles (Si and Al).

Although water sampling captured a range of base-flow conditions between 2013–2016, additional sampling may be needed to document radium transport during high-flow conditions and corresponding annual discharge quantities. Additionally, although sediment samples were collected to shallow depths along downstream transects twice in 2016, repeated sampling at other times and greater depths may be needed to provide high resolution on a temporal scale. The sequential extraction, mineralogical, and geochemical modeling results consistently indicated significant associations between radium and carbonate solids. However, additional work may be appropriate to determine the precise compositions and mineralogy of the relevant phases, including low concentrations of sulfate minerals, if radium is primarily contained within the solid matrix or adsorbed on surfaces, and if identified carbonate (and sulfate) solid solutions remain stable or tend to recrystallize into pure component phases over time or as geochemical conditions vary.

Future studies may be considered to evaluate possible management scenarios to reduce radium transport from the produced water discharge sites. For example, increasing aeration in O&G holding tanks and ponds already in existence could increase dissolved oxygen concentrations, encourage radium adsorption with precipitated iron and manganese oxides, or its coprecipitation into carbonate and sulfate minerals. Aeration of the discharges would tend to increase oxygen concentrations and increase pH, which favors the kinetics of iron and manganese oxidation as well as carbonate precipitation. Additionally, the construction of low energy areas of sediment

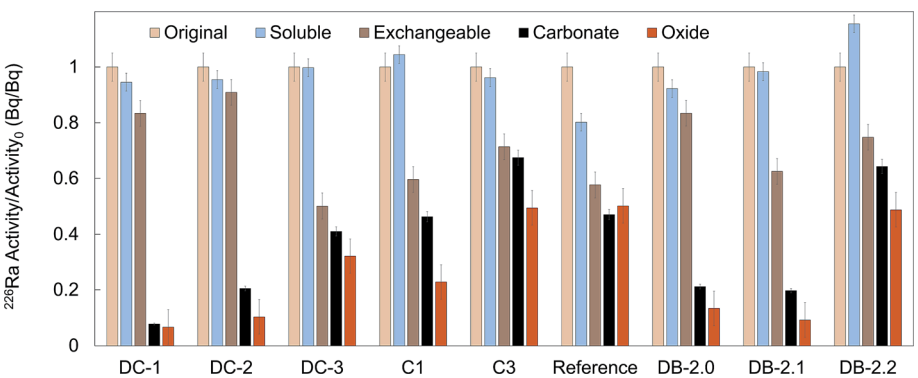

Fig. 7 Radium 226 activity in samples following liquid extraction steps normalized to values of the original sediment. Note the majority of sediments collected near discharge sites contained significantly less radium following extraction steps 2 (exchangeable) and 3 (carbonate). Combined, this indicates the radium is present in and likely associated with easily leachable minerals such as calcium carbonate and not in recalcitrant forms such as sulfates (barite and celestite).

deposition such as in wetland complexes where radium could be sorbed to iron and manganese oxides, buried as carbonate and/or barite solid solution particles, and bioaccumulated in vegetation may be evaluated with consideration of possible impacts to wildlife and livestock. Lastly, various sources of NORM other than O&G extraction activities could be inventoried and evaluated to gain a greater understanding of possible contributions on a regional scale.

Conclusion

The NPDES facilities in this study met dissolved ^{226}Ra effluent regulatory criteria of 2.22 Bq L^{-1} (60 pCi L^{-1}) – both permit-reported and measured. However, lower activities of ^{226}Ra + ^{228}Ra in effluent can still lead to accumulation of high activities of ^{226}Ra + ^{228}Ra in sediments near outfalls, as noted in this and other produced water discharge studies.[5,13,23–25] Sediments at discharges in this study had ^{226}Ra activities nearing 50 times those for background and reference site conditions, whereas values only 5 times background activities exceed action level thresholds. It is important to stress that the sediments studied were not from spill sites but from constant sources of low-level contamination releasing billions of Bq of radium activity to the environment every year.

While the elevated sediment and dissolved radium activities in the water decrease rapidly downstream, the resulting toxicity and health impacts associated with discharges utilized for livestock watering and wildlife propagation remains largely unstudied. Sediment radium accumulation may lead to a long-term ecological footprint when aquatic biota or migratory birds using O&G wetland complexes, permitted as beneficial reuse of produced water, beyond the scope of this study, as flyover habitat are exposed to chronic high sediment radium activities.[1] Agricultural repurposing of produced water may not be justifiable for wildlife propagation where radium accumulates within sensitive organisms (*e.g.*, freshwater mussels) *via* external contact or ingestion, though mortality and growth inhibition effects remain unknown.[69]

Radium coprecipitation with carbonate minerals deduced in this field study of western U.S. produced water discharges would create a reservoir of secondary source contamination. As equilibrium conditions shift with episodic dilution and acidification, the carbonate-associated radium would tend to dissolve. Acidic rainwater and snowmelt runoff thus may release previously sequestered radium back to the water column where it is bioavailable to both animals and humans.[51,57]

Due to the rapid attenuation of Ra towards background activities within short distances downstream of NPDES facilities, but with apparent accumulation in stream sediments that remain mobile, potential solutions to continue beneficial use practices according to 40 CFR § 435 Subpart E from a Ra standpoint could include construction of low-maintenance wetlands/infiltration ponds below points of discharge. This would allow for establishment of collection areas for radium accumulation under chemical and equilibrium conditions (*i.e.* temperature stabilization and increased oxygen concentrations) and reduce transport of radium in the receiving streams. Infrequently, sediments with associated radium could be removed and disposed as appropriate.

Conflicts of interest

There are no conflicts of interest to declare.

Acknowledgements

We gratefully acknowledge Johnna Puhr, Yadiel Varela Soler and Sydney Page for assistance with grab and core sediment preparation, Travis Tasker for analyzing samples with the ICP-AES, and O&G collaborators without whom this project could not have taken place.

References

1 K. Guerra, K. Dahm and S. Dundorf, *Oil and gas produced water management and beneficial use in the Western United States, Science and Technology Program Report No. 157*, US Department of Interior, Bureau of Reclamation, Denver, USA, 2011.
2 F. C. Dolan, T. Y. Cath and T. S. Hogue, Assessing the feasibility of using produced water for irrigation in Colorado, *Sci. Total Environ.*, 2018, **640–641**, 619–628.
3 T. A. Blewett, P. L. M. Delompré, C. N. Glover and G. G. Goss, Physical immobility as a sensitive indicator of hydraulic fracturing fluid toxicity towards Daphnia magna, *Sci. Total Environ.*, 2018, **635**, 639–643.
4 T. A. Blewett, A. M. Weinrauch, P. L. M. Delompré and G. G. Goss, The effect of hydraulic flowback and produced water on gill morphology, oxidative stress and antioxidant response in rainbow trout (Oncorhynchus mykiss), *Sci. Rep.*, 2017, **7**, 46582.
5 N. R. Warner, C. A. Christie, R. B. Jackson and A. Vengosh, Impacts of shale gas wastewater disposal on water quality in Western Pennsylvania, *Environ. Sci. Technol.*, 2013, **47**, 11849–11857.
6 C. D. Kassotis, L. R. Iwanowicz, D. M. Akob, I. M. Cozzarelli, A. C. Mumford, W. H. Orem and S. C. Nagel, Endocrine disrupting activities of surface water associated with a West Virginia oil and gas industry wastewater disposal site, *Sci. Total Environ.*, 2016, **557–558**, 901–910.
7 J. S. Harkness, G. S. Dwyer, N. R. Warner, K. M. Parker, W. A. Mitch and A. Vengosh, Iodide, Bromide, and Ammonium in Hydraulic Fracturing and Oil and Gas Wastewaters: Environmental Implications, *Environ. Sci. Technol.*, 2015, **49**, 1955–1963.
8 K. M. Parker, T. Zeng, J. Harkness, A. Vengosh and W. A. Mitch, Enhanced Formation of Disinfection Byproducts in Shale Gas Wastewater-Impacted Drinking Water Supplies, *Environ. Sci. Technol.*, 2014, **48**, 11161–11169.
9 K. J. Ferrar, D. R. Michanowicz, C. L. Christen, N. Mulcahy, S. L. Malone and R. K. Sharma, Assessment of effluent contaminants from three facilities discharging marcellus

shale wastewater to surface waters in pennsylvania, *Environ. Sci. Technol.*, 2013, **47**, 3472–3481.

10 G. J. Getzinger, M. P. O'Connor, K. Hoelzer, B. D. Drollette, O. Karatum, M. A. Deshusses, P. L. Ferguson, M. Elsner and D. L. Plata, Natural Gas Residual Fluids: Sources, Endpoints, and Organic Chemical Composition after Centralized Waste Treatment in Pennsylvania, *Environ. Sci. Technol.*, 2015, **49**, 8347–8355.

11 M. L. Hladik, M. J. Focazio and M. Engle, Discharges of produced waters from oil and gas extraction *via* wastewater treatment plants are sources of disinfection by-products to receiving streams, *Sci. Total Environ.*, 2014, **466**, 1085–1093.

12 J. M. Wilson and J. M. Van Briesen, Oil and Gas Produced Water Management and Surface Pennsylvania, *Environ. Pract.*, 2012, **14**, 288–301.

13 N. E. Lauer, N. R. Warner and A. Vengosh, Sources of Radium Accumulation in Stream Sediments near Disposal Sites in Pennsylvania: Implications for Disposal of Conventional Oil and Gas Wastewater, *Environ. Sci. Technol.*, 2018, **52**, 955–962.

14 A. Vengosh, *Salinization and Saline Environments*, Elsevier Ltd., 2nd edn, 2013, vol. 11.

15 E. L. Rowan, M. A. Engle, C. S. Kirby and T. F. Kraemer, *Radium Content of Oil- and Gas-Field Produced Waters in the Northern Appalachian Basin (USA): Summary and Discussion of Data*, U.S. Geological Survey Sci. Investig. Rep., 2011, p. 38.

16 K. Oetjen, J. Blotevogel, T. Borch, J. F. Ranville and C. P. Higgins, Simulation of a hydraulic fracturing wastewater surface spill on agricultural soil, *Sci. Total Environ.*, 2018, **645**, 229–234.

17 United Nations, *Sources and Effects of Ionizing Radiation United Nations Scientific Committee on the Effects of Atomic Radiation*, New York, 2011, vol. II.

18 F. Carvalho, D. Chambers, S. Fesenko, W. S. Moore, D. Porcelli, H. Vandenhoven and T. Yankovich, *Environmental Pathways and Corresponding Models*, Vienna, 2014.

19 National Research Council, *Health Effects of Exposure to Radon*, National Academies Press, 1999.

20 US Nuclear Regulatory Commission, *Appendix B to Part 20 Annual Limits on Intake (ALIs) and Derived Air Concentrations (DACs) of Radionuclides for Occupational Exposure; Effluent Concentrations*, Concentrations for Release to Sewerage, 2017.

21 US Environmental Protection Agency, *National Interim Primary Drinking Water Regulations*, Washington, DC, 1976.

22 J. Rosenblum, A. W. Nelson, B. Ruyle, M. K. Schultz, J. N. Ryan and K. G. Linden, Temporal characterization of flowback and produced water quality from a hydraulically fractured oil and gas well, *Sci. Total Environ.*, 2017, **596–597**, 369–377.

23 W. D. Burgos, L. Castillo-Meza, T. L. Tasker, T. J. Geeza, P. J. Drohan, X. Liu, J. D. Landis, J. Blotevogel, M. McLaughlin, T. Borch and N. R. Warner, Watershed-Scale Impacts from Surface Water Disposal of Oil and Gas Wastewater in Western Pennsylvania, *Environ. Sci. Technol.*, 2017, **51**, 8851–8860.

24 I. M. Cozzarelli, K. J. Skalak, D. B. Kent, M. A. Engle, A. Benthem, A. C. Mumford, K. Haase, A. Farag, D. Harper, S. C. Nagel, L. R. Iwanowicz, W. H. Orem, D. M. Akob, J. B. Jaeschke, J. Galloway, M. Kohler, D. L. Stoliker and G. D. Jolly, Environmental signatures and effects of an oil and gas wastewater spill in the Williston Basin, North Dakota, *Sci. Total Environ.*, 2016, **579**, 1781–1793.

25 N. E. Lauer, J. S. Harkness and A. Vengosh, Brine Spills Associated with Unconventional Oil Development in North Dakota, *Environ. Sci. Technol.*, 2016, **50**, 5389–5397.

26 International Atomic Energy Agency, *The Environmental Behaviour of Radium*, revised edn, Vienna, 2014.

27 C. A. Menzie, B. Southworth, G. Stephenson and N. Feisthauer, The importance of understanding the chemical form of a metal in the environment: The case of barium sulfate (barite), *Hum. Ecol. Risk Assess.*, 2008, **14**, 974–991.

28 B. Ouyang, D. M. Akob, D. Dunlap and D. Renock, Microbially mediated barite dissolution in anoxic brines, *Appl. Geochem.*, 2017, **76**, 51–59.

29 D. Renock, J. D. Landis and M. Sharma, Reductive weathering of black shale and release of barium during hydraulic fracturing, *Appl. Geochem.*, 2016, **65**, 73–86.

30 E. R. Elizabeth and J. P. Phillips, Sulfate-Reducing Bacteria Release Barium and Radium from Naturally Occurring Radioactive Material in Oil-Field Barite, *Geomicrobiol. J.*, 2001, **18**, 167–182.

31 K. Van Sice, C. A. Cravotta, B. McDevitt, T. L. Tasker, J. Landis, J. Puhr and N. R. Warner, Radium fate following oil and gas wastewater disposal to western Pennsylvania surface waters, *Appl. Geochem.*, 2018, **98**, 393–403.

32 T. Zhang, K. Gregory, R. W. Hammack and R. D. Vidic, Co-precipitation of radium with barium and strontium sulfate and its impact on the fate of radium during treatment of produced water from unconventional gas extraction, *Environ. Sci. Technol.*, 2014, **48**, 4596–4603.

33 T. Zhang, R. W. Hammack and R. D. Vidic, Fate of Radium in Marcellus Shale Flowback Water Impoundments and Assessment of Associated Health Risks, *Environ. Sci. Technol.*, 2015, **49**, 9347–9354.

34 M. Sajih, N. D. Bryan, F. R. Livens, D. J. Vaughan, M. Descostes, V. Phrommavanh, J. Nos and K. Morris, Adsorption of radium and barium on goethite and ferrihydrite: A kinetic and surface complexation modelling study, *Geochim. Cosmochim. Acta*, 2014, **146**, 150–163.

35 A. Vengosh, R. B. Jackson, N. Warner, T. H. Darrah and A. Kondash, A critical review of the risks to water resources from unconventional shale gas development and hydraulic fracturing in the United States, *Environ. Sci. Technol.*, 2014, **48**, 8334–8348.

36 A. J. Kondash, N. R. Warner, O. Lahav and A. Vengosh, Radium and barium removal through blending hydraulic fracturing fluids with acid mine drainage, *Environ. Sci. Technol.*, 2014, **48**, 1334–1342.

37 F. Grandia, J. Merino and J. Bruno, *Assessment of the radium-barium co-precipitation and its potential influence on the solubility of Ra in the near-field*, 2008, vol. TR-08-07, p. 52.

38 C. He, M. Li, W. Liu, E. Barbot and R. D. Vidic, Kinetics and Equilibrium of Barium and Strontium Sulfate Formation in Marcellus Shale Flowback Water, *J. Environ. Eng.*, 2014, **140**(5), DOI: 10.1061/(asce)ee.1943-7870.0000807.

39 D. Langmuir and D. Melchior, The geochemistry of Ca, Sr, Ba and Ra sulfates in some deep brines from the Palo Duro Basin, Texas, *Geochim. Cosmochim. Acta*, 1985, **49**, 2423–2432.

40 F. Brandt, E. Curti, M. Klinkenberg, K. Rozov and D. Bosbach, Replacement of barite by a (Ba,Ra)SO_4 solid solution at close-to-equilibrium conditions: A combined experimental and theoretical study, *Geochim. Cosmochim. Acta*, 2015, **155**, 1–15.

41 V. L. Vinograd, F. Brandt, K. Rozov, M. Klinkenberg, K. Refson, B. Winkler and D. Bosbach, Solid-aqueous equilibrium in the $BaSO_4$–$RaSO_4$–H_2O system: First-principles calculations and a thermodynamic assessment, *Geochim. Cosmochim. Acta*, 2013, **122**, 398–417.

42 V. L. Vinograd, D. A. Kulik, F. Brandt, M. Klinkenberg, J. Weber, B. Winkler and D. Bosbach, Thermodynamics of the solid solution – Aqueous solution system (Ba,Sr,Ra)SO_4 + H_2O: I. The effect of strontium content on radium uptake by barite, *Appl. Geochem.*, 2018, **89**, 59–74.

43 V. L. Vinograd, D. A. Kulik, F. Brandt, M. Klinkenberg, J. Weber, B. Winkler and D. Bosbach, Thermodynamics of the solid solution – Aqueous solution system (Ba,Sr,Ra)SO_4 + H_2O: II. Radium retention in barite-type minerals at elevated temperatures, *Appl. Geochem.*, 2018, **93**, 190–208.

44 A. J. Tesoriero and J. F. Pankow, Solid solution partitioning of Sr^{2+}, Ba^{2+}, and Cd^{2+} to calcite, *Geochim. Cosmochim. Acta*, 1996, **60**, 1053–1063.

45 E. Curti, Coprecipitation of radionuclides with calcite: Estimation of partition coefficients based on a review of laboratory investigations and geochemical data, *Appl. Geochem.*, 1999, **14**, 433–445.

46 D. S. Vinson, J. R. Lundy, G. S. Dwyer and A. Vengosh, Implications of carbonate-like geochemical signatures in a sandstone aquifer: Radium and strontium isotopes in the Cambrian Jordan aquifer (Minnesota, USA), *Chem. Geol.*, 2012, **334**, 280–294.

47 W. Back and B. B. Hanshaw, Comparison of chemical hydrogeology of the carbonate peninsulas of Florida and Yucatan, *J. Hydrol.*, 1970, **10**, 330–368.

48 P. Glynn, Solid-Solution Solubilities and Thermodynamics: Sulfates, Carbonates and Halides, *Rev. Mineral. Geochem.*, 2000, **40**, 481–511.

49 B. B. Hanshaw and W. Back, Major geochemical processes in the evolution of carbonate-aquifer systems, *Dev. Water Sci.*, 1979, **12**, 287–312.

50 M. J. Jones, L. J. Butchins, J. M. Charnock, R. A. D. Pattrick, J. S. Small, D. J. Vaughan, P. L. Wincott and F. R. Livens, Reactions of radium and barium with the surfaces of carbonate minerals, *Appl. Geochem.*, 2011, **26**, 1231–1238.

51 P. M. Dove and F. M. Platt, Compatible real-time rates of mineral dissolution by Atomic Force Microscopy (AFM), *Chem. Geol.*, 1996, **127**, 331–338.

52 C. Clark and J. Veil, *U.S. Produced water volumes and management practices*, Groundw. Prot. Counc., 2015, p. 119.

53 US Environmental Protection Agency, *Rapid Radiochemical Methods for Selected Radionuclides in Water for Environmental Restoration Following Homeland Security Events*, Montgomery, 2010.

54 US Environmental Protection Agency, *Radiochemistry Procedures Manual*, 1984.

55 N. Lauer and A. Vengosh, Age Dating Oil and Gas Wastewater Spills Using Radium Isotopes and Their Decay Products in Impacted Soil and Sediment, *Environ. Sci. Technol. Lett.*, 2016, **3**, 205–209.

56 B. W. Stewart, E. C. Chapman, R. C. Capo, J. D. Johnson, J. R. Graney, C. S. Kirby and K. T. Schroeder, Origin of brines, salts and carbonate from shales of the Marcellus Formation: Evidence from geochemical and Sr isotope study of sequentially extracted fluids, *Appl. Geochem.*, 2015, **60**, 78–88.

57 T. T. Phan, R. C. Capo, B. W. Stewart, J. R. Graney, J. D. Johnson, S. Sharma and J. Toro, Trace metal distribution and mobility in drill cuttings and produced waters from Marcellus Shale gas extraction: Uranium, arsenic, barium, *Appl. Geochem.*, 2015, **60**, 89–103.

58 D. L. Parkhurst and C. A. J. Appelo, Description of Input and Examples for PHREEQC Version 3—A Computer Program for Speciation, Batch-Reaction, One-Dimensional Transport, and Inverse Geochemical Calculations, *U.S. Geological Survey Techniques and Methods,* 2013, vol. 6, ch. 43A, p. 497.

59 J. W. Ball and D. K. Nordstrom, *User's Manual for Wateq4F, With Revised Thermodynamic Data Base and Test Cases for Calculating Speciation of Major, Trace, and Redox Elements in Natural Waters*, U.S. Geol. Surv., open-file rep. 91-183, 1991.

60 E. Giffaut, M. Grivé, P. Blanc, P. Vieillard, E. Colàs, H. Gailhanou, S. Gaboreau, N. Marty, B. Madé and L. Duro, Andra thermodynamic database for performance assessment: ThermoChimie, *Appl. Geochem.*, 2014, **49**, 225–236.

61 D. Langmuir and A. C. Riese, The Thermodynamic Properties of Radium, *Geochim. Cosmochim. Acta*, 1985, **49**, 1593–1601.

62 R. B. McCleskey, D. K. Nordstrom, J. N. Ryan and J. W. Ball, A new method of calculating electrical conductivity with applications to natural waters, *Geochim. Cosmochim. Acta*, 2012, **77**, 369–382.

63 Y. O. Rosenberg, Z. Sade and J. Ganor, The precipitation of gypsum, celestine, and barite and coprecipitation of radium during seawater evaporation, *Geochim. Cosmochim. Acta*, 2018, **233**, 50–65.

64 R. M. Rodríguez-Galán and M. Prieto, Interaction of Nonideal, Multicomponent Solid Solutions With Water: A Simple Algorithm to Estimate Final Equilibrium States, *Geochem., Geophys., Geosyst.*, 2018, **19**, 1348–1359.

65 P. Dresel and A. Rose, Chemistry and origin of oil and gas well brines in western Pennsylvania, Pennsylvania Geol. Surv., 4th ser., open-file rep. OFOG 10–01.0, 2010, p. 48.

66 D. Barišić, S. Lulić and P. Miletić, Radium and uranium in phosphate fertilizers and their impact on the radioactivity of waters, *Water Res.*, 1992, **26**, 607–611.
67 W. S. Moore, J. L. Sarmiento and R. M. Key, Submarine groundwater discharge revealed by ^{228}Ra distribution in the upper Atlantic Ocean, *Nat. Geosci.*, 2008, **1**, 309–311.
68 P. J. Ramirez, *Oil Field Produced Water Discharges into Wetlands in Wyoming*, US Fish and Wildlife Service Environmental, contamination report R6/718C/02, 2015.
69 T. J. Geeza, D. P. Gillikin, B. McDevitt, K. Van Sice and N. R. Warner, Accumulation of Marcellus Formation Oil and Gas Wastewater Metals in Freshwater Mussel Shells, *Environ. Sci. Technol.*, 2018, **52**, 10883–10892.
70 P. Benes, Z. Borovec and P. Strejc, Interaction of Radium With Freshwater Sediments and their Mineral Components: III. Muscovite and Feldspar, *J. Radioanal. Nucl. Chem.*, 1986, **98**, 91–103.
71 P. Benes, P. Strejc and Z. Lukavec, Interaction of Radium with Freshwater Sediments and their Mineral Components. I.Ferric hydroxide and quartz, *J. Radioanal. Nucl. Chem.*, 1984, **82**, 275–285.

